



Spectroscopic studies, molecular structure optimization and investigation of structural and electrical properties of novel and biodegradable Chitosan-GO polymer nanocomposites

Vimala Dhayal¹, S. Z. Hashmi², Upendra Kumar¹, B. L. Choudhary¹, A. E. Kuznetsov³, Saurabh Dalela⁴, Shalendra Kumar⁵, Savas Kaya⁶, S. N. Dolia⁷, and P. A. Alvi^{1,*}

¹Department of Physics, Banasthali Vidyapith, Banasthali, Rajasthan 304022, India

²Department of Chemistry, Banasthali Vidyapith, Banasthali, Rajasthan 304022, India

³Departamento de Química, Universidad Tecnica Federico Santa María, Av. Santa María 6400 Vitacura, 7660251 Santiago, Chile

⁴Department of Pure & Applied Physics, University of Kota, Kota, Rajasthan 324005, India

⁵Department of Physics, College of Science, King Faisal University, P.O. Box 400, Hofuf 31982, Al-Ahsa, Saudi Arabia

⁶Department of Chemistry, Cumhuriyet University, Sivas, Turkey

⁷Department of Physics, University of Rajasthan, Jaipur, Rajasthan 302004, India

Received: 21 April 2020

Accepted: 5 July 2020

Published online:

27 July 2020

© Springer Science+Business Media, LLC, part of Springer Nature 2020

ABSTRACT

This article covers the molecular structure optimization and spectroscopic studies, such as Raman, UV–Vis absorption and FTIR, carried out for novel, biodegradable and biocompatible chitosan-graphene oxide (CS-GO) polymer nanocomposites (PNCs), which were synthesized by using simple blending technique followed by ultrasonification treatment. In addition, the structural and electrical properties have also been investigated. Under molecular structure optimization, the structural geometry, electronic structure (HOMO and LUMO) and potential distribution have been computed. X-ray diffraction of PNCs reveals that the crystallized phase of GO dominates over the CS giving modification in crystallite size and presence of micro-strain. FTIR and Raman spectroscopic studies have been carried out to confirm the proper formation of PNCs and presence of functional group in the composites. The surface morphology has been studied with the help of FESEM to confirm proper dispersion of GO sheets. Optical absorption edge and band gap analyzed from UV–Vis analysis reveal the semiconducting nature of PNCs. In addition, the optical band gap is tuned by varying the content of GO in PNCs. This tuning in band gap has also been supported by XRD and computational results. The dielectric constant and dc conductivity are found increased with increasing content of GO in PNCs. Additionally, the I–V characteristics of PNCs shows Ohmic type conduction

Address correspondence to E-mail: drpaalvi@gmail.com

with rising in current due to incorporation of GO. In view of the results achieved, the usage of CS-GO PNC is suitable for future development of optical and Gas sensors and UV-detectors, and therefore, such composite may be proven as a potential and suitable candidate for the optoelectronic or electrical devices operating at high frequencies.

Introduction

In the last two decades, an interest has been grown to develop polymer-based nanomaterials and nanocomposites, which have technological importance in diverse areas such as sensors, electronic and optoelectronic devices, pharmaceuticals, food packaging, biological and medical applications [1–6]. In addition, such materials have also been utilized successfully in the environmental conservation and protection [7]. Specifically, 2-D nanomaterials such a graphene and its derivatives as effective nano-fillers in combination with the polymer matrix have made them advanced polymer nanocomposite materials, which can led to many advanced applications [8,9]. However, moving toward specific nanocomposites being fully biodegradable and environment-friendly and hence considered as 'green' composites synthesized from the plant fibers and resins is important. These are developed for diverse applications and are alternatives for non-degradable materials derived from petroleum. In order to synthesize such nanomaterials or nanocomposites, the biopolymer or natural polymer plays a very important role. Chitosan is one of the natural, non-toxic, biocompatible and biodegradable polymers which have significantly contributed in sustainable development and other potential applications [10]. Moreover, due to the biodegradability in environment and biocompatibility, such novel and biocompatible materials-based nanocomposites have drawn a great attention of researchers for their successful usage in many areas of science and technology. In case of such nanocomposites, the polymer matrix and the nanomaterials or nanoparticles make their successful contribution in order to enhance their specific properties [11]. The chitosan (CS)-based nanocomposites are one of them. The major utility of chitosan-based nanocomposites, due to their non-toxic behavior, is in food packaging, nano-coatings and other medical application [12,13]. This is because the chitosan has transparent film forming quality. Further, being non-toxic,

biocompatible and biodegradable, it can be used as a potential biomaterial. Due to its ability to bind with cholesterol, metal ions and fats, it can also be used as a chelating agent. The amino group present in it might be protonated providing it a positive charge making it soluble in dilute acidic aqueous solutions. Chitosan being positively charged can interact with the negative part of the cell membrane leading to the reorganization and opening of tight protein junctions making it permeable.

Generally, the chitosan-based polymer nanocomposites (PNCs) are formed between chitosan (as polymer matrix) and metal oxide or carbon materials (as nano-fillers) via physical or chemical interaction. Specifically, when the CS-based PNCs are prepared using metal oxide (MO) nano-fillers, the antimicrobial and mechanical properties of CS are enhanced, and therefore, the CS-MO PNCs are utilized in food packaging, food preservation applications and mainly in coatings [14]. Moreover, the other nano-fillers like magnetite (Fe_3O_4) nanoparticles with super-paramagnetic monodispersion behavior into the conjugated polymers such as poly(3, 4-ethylene-dioxythiophene) (PEDOT) and conducting polymer like sulfonated polyaniline, [poly(aniline-co-8-amino-2-naphthalenesulfonic acid) PANSA] and sulfonated polyaniline, poly(aniline-co-aminonaphthalenesulfonic acid) [SPAN(ANSA)] have been investigated [15–20]. Similarly, the MO nano-fillers have been claimed to enhance the sensitivity and stability of the conductive polymer matrix such as polyaniline, polypyrrole, polythiophene and their derivatives to make these polymers suitable for applications in amperometric sensors and biosensors [21].

However, the CS-based PNCs by using carbon and their derivatives such as carbon nanotubes, graphene, graphene oxide (GO) and r-GO (reduced graphene oxide) as nano-fillers have opened a wide opportunities in various scientific areas, because the usage of these nano-fillers in CS based PNCs has exhibited outstanding properties such as high mechanical strength, high molecular barrier abilities, good

electrical conductivity and easily dispersible with polymer or ceramic matrixes to enhance their mechanical and electrical properties, even with a small quantity of nano-fillers [22–24]. As reported in previous literature, the functionalized MWCNTs (multi-walled carbon nanotubes) along with the noble metal nanoparticles as nano-fillers have been incorporated into the conducting polyaniline polymer matrix. The synthesized hybrid CNTs–polymer/metal nanocomposites have been claimed in numerous applications in nanotechnology, gas sensing and catalysis [25]. Similarly, the CNT composites in a colloidal system with poly(styrene) have been synthesized to prepare the nanostructured brush [26]. Further, as compared to the conventional nano-fillers, GO (as nano-filler) has been a milestone for the advanced PNCs. The reason behind its role in the PNCs is its unique and remarkable chemical, physical, mechanical, electrical and electronic properties [27–32]. For example, Kim et al. have fabricated a flexible super-capacitor by using polyaniline/r-GO PNC and showed the capacitance of order of 431 F/g [33]. The electrical conductivity for polyaniline/r-GO PNC was measured as $\sim 9.06 \times 10^4$ S/m. Similarly, the graphene/polyaniline nanostructures have been synthesized to form the free-standing supercapacitor electrode [34]. Apart from these properties, the other important features are fire retardants of epoxy resin [35], compatibility of thermally reduced r-GO with polyesters [36], lipophilicity under special treatment [37], stable aqueous colloidal dispersions [38] and the molecular barrier ability [39], which occurs due to the high packing density of sp^2 carbon atoms. Such tight packing between the carbon atoms is served as an almost-perfect barrier to the flow of gas molecules. Other application may be as corrosion-resistant material which can be used as protective materials for sensitive electronic or flexible optoelectronic devices [40,41]. Apart from these applications of the polymer nanocomposites, the major contribution have been made in the direction of energy storage devices such as polymer composites based lithium and sodium-ion batteries [42–47], in fuel cells [48] and in removing heavy metals [49].

Experimental detail

Materials

For the synthesis of CS-GO polymer nanocomposites, GO as nano-filler (with purity > 99%, diameter 0.82 nm and length 5–10 μm) and chitosan as polymer matrix in powder form (soluble in aqueous acetic acid) were purchased from Sigma-Aldrich Chemical Co., New Delhi, India (USA origin). The dispersing media such as acetic acid and deionized water were purchased from the Merck New Delhi, India (USA origin). However, the acetone used for cleaning purpose was also procured from Merck.

Methods

In order to seek the potential applications of CS-GO PNCs in the area of pharmacy, food packaging, biological, medical, optical, electronics and optoelectronics applications, particularly in flexible electronics, the structural, FTIR (Fourier transform infrared), Raman bands, surface morphology, optical (optical absorption spectra and optical band gaps), electrical properties (i.e., dissipation factor, dielectric loss, etc.) and I–V characteristics of CS-GO PNCs have been studied by using X-ray diffractometer, IR spectrophotometer, Raman spectrometer, FESEM (Field emission scanning electron microscope), UV–Vis spectro-photometer, impedance analyzer and Keithly Source meter, respectively. Hopefully, the work carried out is totally applications oriented and definitely the results achieved will be useful for various applications of novel and eco-friendly CS-GO nanocomposites.

Synthesis process

At initial step, GO was dispersed in an aqueous solution of acetic acid with the help of a sonicator. After that, the dispersed GO was poured into the prepared solution of chitosan, which was prepared into the mixture of deionized water (100 ml) and acetic acid (0.5 g). This final mixture was kept on the magnetic stirrer system at normal temperature for 24 h. In order to ensure the homogeneity of the prepared solution of chitosan and GO, the stirred solution was passed through an ultrasonication bath treatment. Thus, the final mixed solution was poured and cast on a glass disk to a desired thickness (by

spinning casting) in order to achieve CS-GO polymer nanocomposites in the form of freestanding films and dried at room temperature for about two days. For 1 wt% GO, 2 wt% GO, 3 wt% GO and 4 wt% GO, the real contents of GO were taken as 0.005 g, 0.01 g, 0.015 g and 0.020 g in 0.5 g CS polymer matrix, respectively.

The flowchart for the synthesis procedure of CS-GO polymer nanocomposites is illustrated in Fig. 1, and the synthesized free standing film of CS-GO PNC is shown in Fig. 2. The four samples were prepared with the different GO concentrations, i.e., 1, 2, 3 and 4 wt% of GO. The growth of polymer nano-composites can be understood by nucleation and growth process, in which, when a solid polymer is dispersed into a liquid medium, this is transformed to fine size particle, called nucleus. Thereafter, this nucleus is settled to the medium and other similar fine particles are attached to the outer surface of that nucleus in different orientation, called growth. In growth process, the Gibbs energy ($\Delta G \leq 0$) plays a crucial role to form a grain or a crystalline phase. The size of the grain or crystal structure up to the satisfaction of this criterion is called critical size.

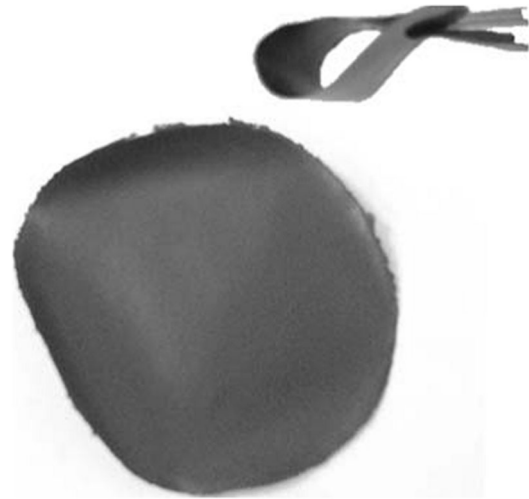


Figure 2 Photograph of prepared freestanding film of CS-GO polymer nanocomposites.

Computational detail for molecular structure optimization

In order to optimize the chemical structure of the CS-GO PNCs, the calculations were performed using the Gaussian 09 package, revision B.01 [50]. For all calculations, the hybrid functional B3LYP [51,52] with the split-valence 6-31G* basis set (B3LYP/6-31G* approach) was employed in the gas phase [53,54]. The structures were optimized without any symmetry constraints and checked for imaginary

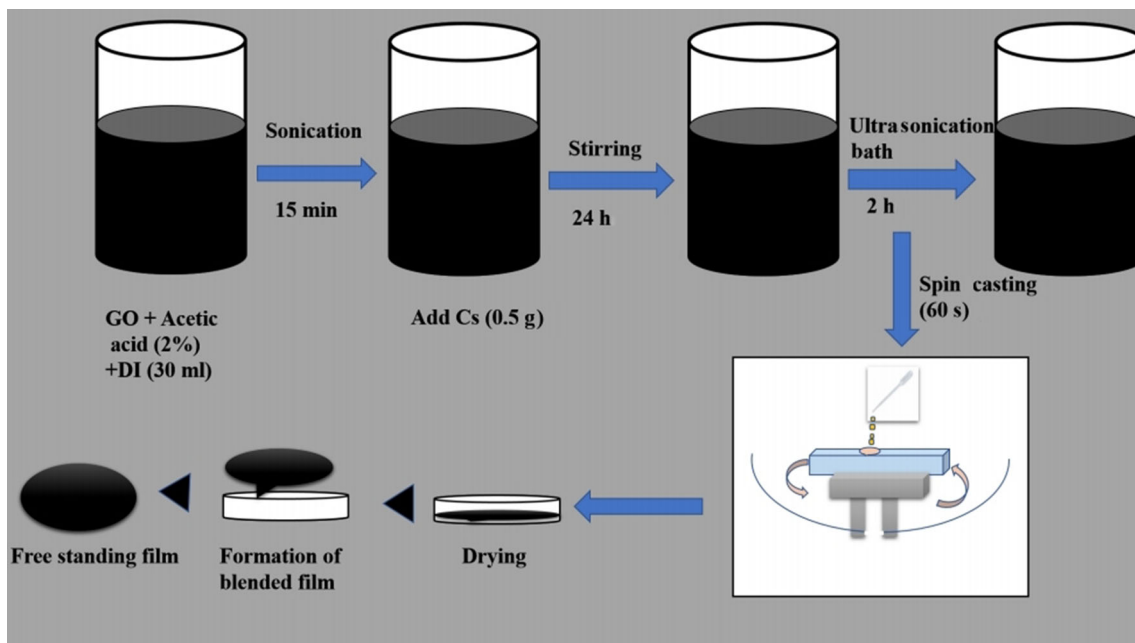


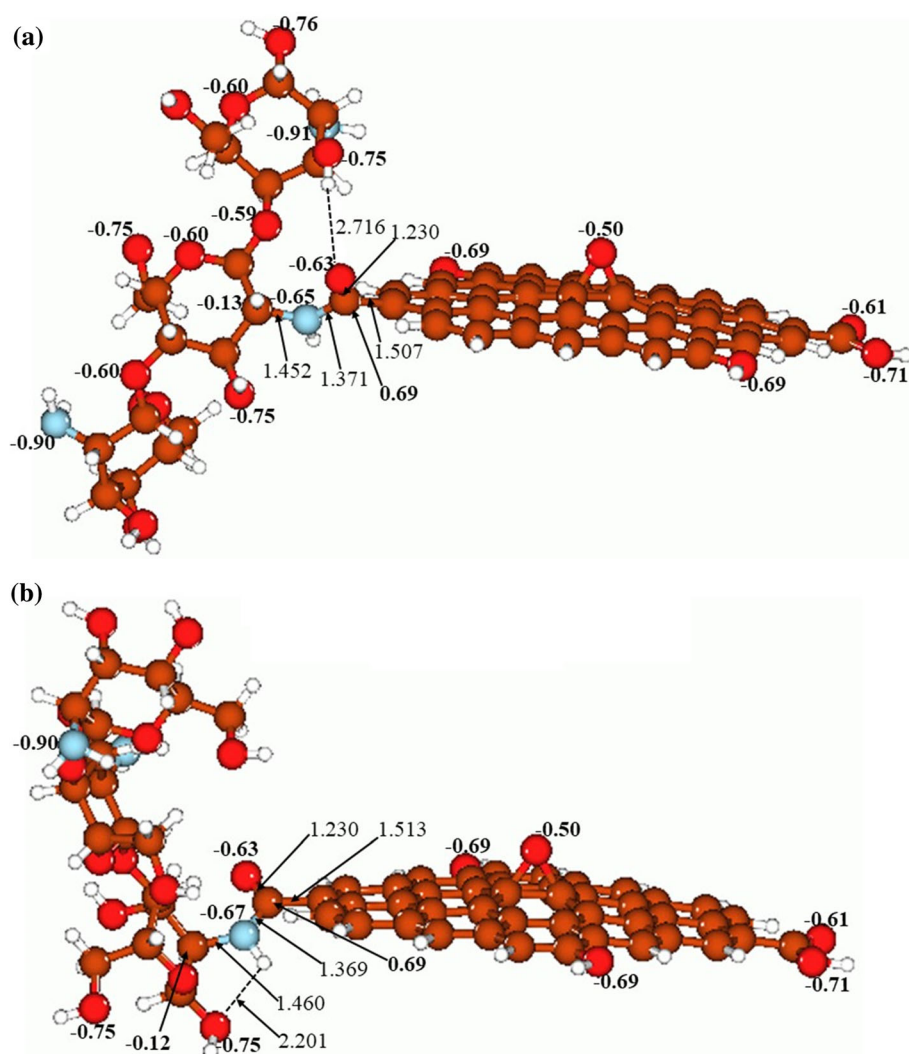
Figure 1 Flowchart for synthesis procedure of CS-GO polymer nanocomposites.

frequencies using vibrational frequency analysis. The charge distribution analysis was performed using the natural bond orbital (NBO) scheme with the ‘pop = nbo’ command as implemented in the Gaussian 09 package [55,56]. Molecular orbitals (MOs) and molecular electrostatic potential (MEP) were calculated at the B3LYP/6-31G* level in the gas phase on the B3LYP/6-31G* optimized geometries. Molecular structures and molecular orbitals were visualized using OpenGL version of Molden 5.8.2 visualization software [57]. MEP results were visualized using the Avogadro software [58,59].

For our calculations, we used the $C_{42}H_{12}(OH)_2(-CO_2H)_2(=O)$ model for graphene oxide (GO) and the oligomer with three monomeric units for chitosan (CS). Two modes of binding between the CS and GO were studied: (1) with the end monomer unit bound through the amide bond to the GO model and (2)

with the middle unit bound through the amide bond to the GO model. Both binding modes give the structures quite close in energy; at the B3LYP/6-31G* level in the gas phase the structure with the mode I was calculated to be 4.19 kcal/mol higher in energy than the structure with the mode II. As once can be seen from Fig. 3, different binding modes of the CS to GO do not influence significantly the geometry of the connecting amide group. The C(CS)–N in the mode II is elongated by mere 0.008 Å (Fig. 3b). The CS moiety itself with the binding mode II becomes noticeably distorted compared to the binding mode I. Also, in both cases the CS moiety and the amide group are formed: in the mode I between the –C=O part of the amide and one of the O–H groups of the end CS ring, with the O···H distance 2.716 Å; in the mode II between the –N–H part of the amide and one of the O–H groups of the same end CS ring, with the much

Figure 3 Structures with two studied modes of binding between CS and GO: **a** with the middle CS model unit bound to the GO, **b** with the end CS model unit bound to the GO. Color coding: brown for C, white for H, red for O, light blue for N. Selected distances are given in Å. Selected NBO charges, e, are given in bold.



shorter O...H distance 2.201 Å. Thus, we can suppose that upon binding to the GO, chitosan might be able to form hydrogen bonds with different O-containing groups on the GO surface and with amide groups, too. Comparing of the selected NBO charges between two binding modes shows them to be essentially the same.

Furthermore, comparison of the frontier MOs for both structures shows their close similarity (Fig. 4). For both structures, both HOMO and LUMO are composed dominantly of the GO contributions, with very small contributions of the amide O-atom in the LUMO in the structure I and in the HOMO in the structure II. However, energies of the MOs differ for both structures: in the lower-energy structure with the binding mode II HOMO and LUMO are *destabilized* compared to the higher-lying structure. However, the HOMO–LUMO gap in the lower-lying structure is *smaller* compared to the higher-energy structure, 2.97 eV compared to 3.01 eV.

Figure 5 shows the MEP maps for both structures. As it can be seen, they are essentially quite similar, with electron density accumulation on O- and N-atoms (red color) and electron density depletion on H-atoms connected to those electronegative atoms (blue color).

Characterizations of CS-GO nanocomposites

In order to characterize the synthesized CS-GO PNC samples, the X-ray diffractometer (XRD), IR spectrophotometer, Raman spectrometer, UV–Vis–NIR spectrophotometer and impedance analyzer were used for the structural analysis, analysis of functional group along with their modes, molecular analysis, analysis of optical properties and electrical properties, respectively.

Structural analysis

The structural analysis of the prepared samples was performed with the help of the XRD (Bruker model-Advance D-8). The X-ray diffraction patterns of prepared CS-GO PNCs are shown in Fig. 6. Here, in the polymer matrix of chitosan, the content of nano-filler GO was increased from 1 to 4 wt%. The XRD patterns of the prepared nanocomposites show hump like peaks, which might be due to the smaller crystallite size of PNCs. Since the synthesis of CS-GO PNCs has been carried out by a simple blending technique, the peaks related to the both phases chitosan and GO should be present in the XRD patterns. The diffraction pattern of chitosan and GO is slight different because of their existence in amorphous and crystalline phase, respectively. With increasing the GO content in CS polymer matrix, the diffraction peaks belonging to the GO become sharper while CS

Figure 4 Frontier molecular orbitals for the structures with binding modes I (a) and II (b).

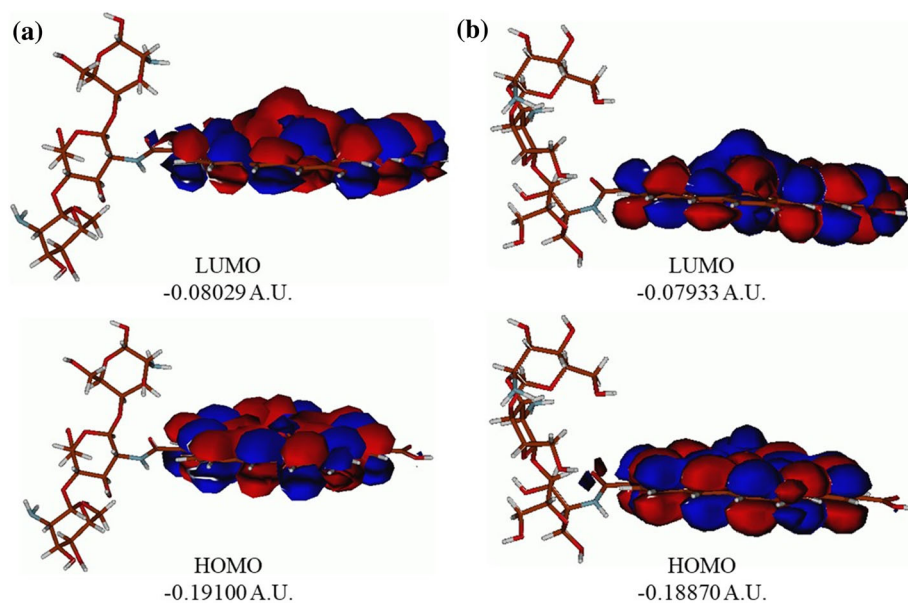


Figure 5 Molecular electrostatic potential (MEP) maps for the structures with binding modes I (a) and II (b).

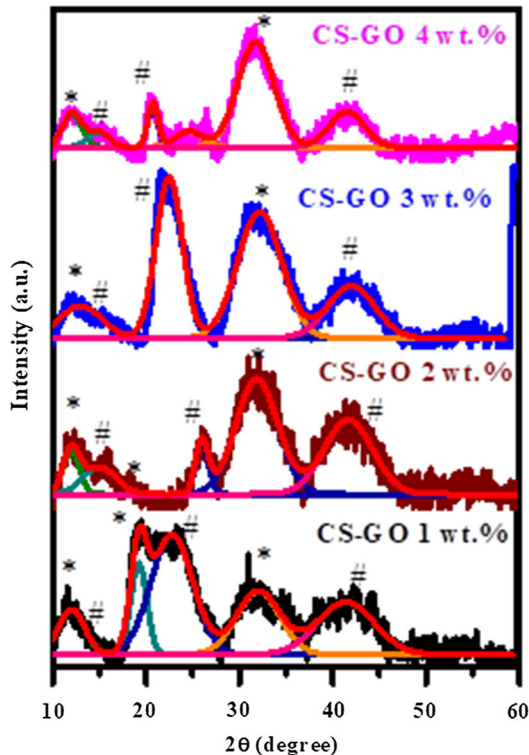
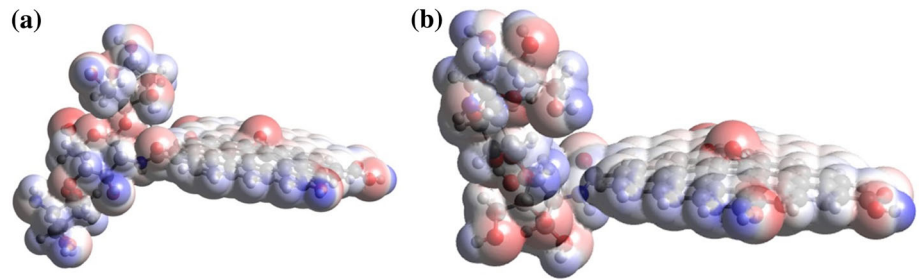


Figure 6 XRD pattern of prepared freestanding films of CS-GO polymer nanocomposites.

become broader. Since the XRD pattern of PNCs is showing hump like peaks, to identify the peaks the XRD pattern was fitted with Gaussian peaks. Further, the presence of chitosan and GO in the XRD pattern was indexed by * and #, respectively.

However, it is noticed that with increasing the content of GO in PNCs, the XRD peaks related to CS become more intense rather than GO because of the strong crystalline nature of GO, while chitosan exhibits semi-crystalline character. The position of XRD peaks related to chitosan and GO is well-matched with the reported literature [60,61]. The broadening in the XRD peak is present due to the contribution of smaller crystallite size as well as micro-strain in the sample. The total width of the peak, also termed as

the full width at half maxima (FWHM), has been written as the sum of FWHM arises due to contribution crystallite size (β_D) and micro-strain (β_ϵ) as the following equation:

$$\beta_{\text{total}} = \beta_D + \beta_\epsilon \tag{1}$$

According to Debye the FWHM of the peak is inversely proportional to the crystallite size and given by equation [62]:

$$\beta_D = \frac{k\lambda}{D\cos\theta} \tag{2}$$

However, the micro-strain in the unit cell can be related to the FWHM of the peak as:

$$\beta_\epsilon = \epsilon \tan \theta \tag{3}$$

Using Eq. (2) and (3) in Eq. (1) the resulting equation can be transformed as follows:

$$\beta_{\text{total}} = \frac{k\lambda}{D\cos\theta} + \epsilon \tan \theta \tag{4}$$

Equation (4) is also called as Williamson–Hall (W–H) plot, and further Eq. (4) has been generalized as follows [63]:

$$\beta_{\text{total}} \cos \theta = \frac{k\lambda}{D} + \epsilon \sin \theta \tag{5}$$

For all samples, the W–H plots have been generated and shown in Fig. 7. The experimental data of samples show a straight line ($y = mx + c$) having slope ($m = \epsilon$) and intercept ($c = \frac{k\lambda}{D}$). Using the value of intercept and slope for all samples, the crystallite size and micro-strain have been calculated and given in Table 1.

The calculated value of crystallite size and micro-strain in CS-GO PNCs, as given in Table 1, is found to be enlarged with increasing GO wt%. In further explanation, as the content of nano-filler increases, the crystallization of the matrix promotes via the nucleation and growth process well explained in the literature [64,65]. In the present study, the filler GO

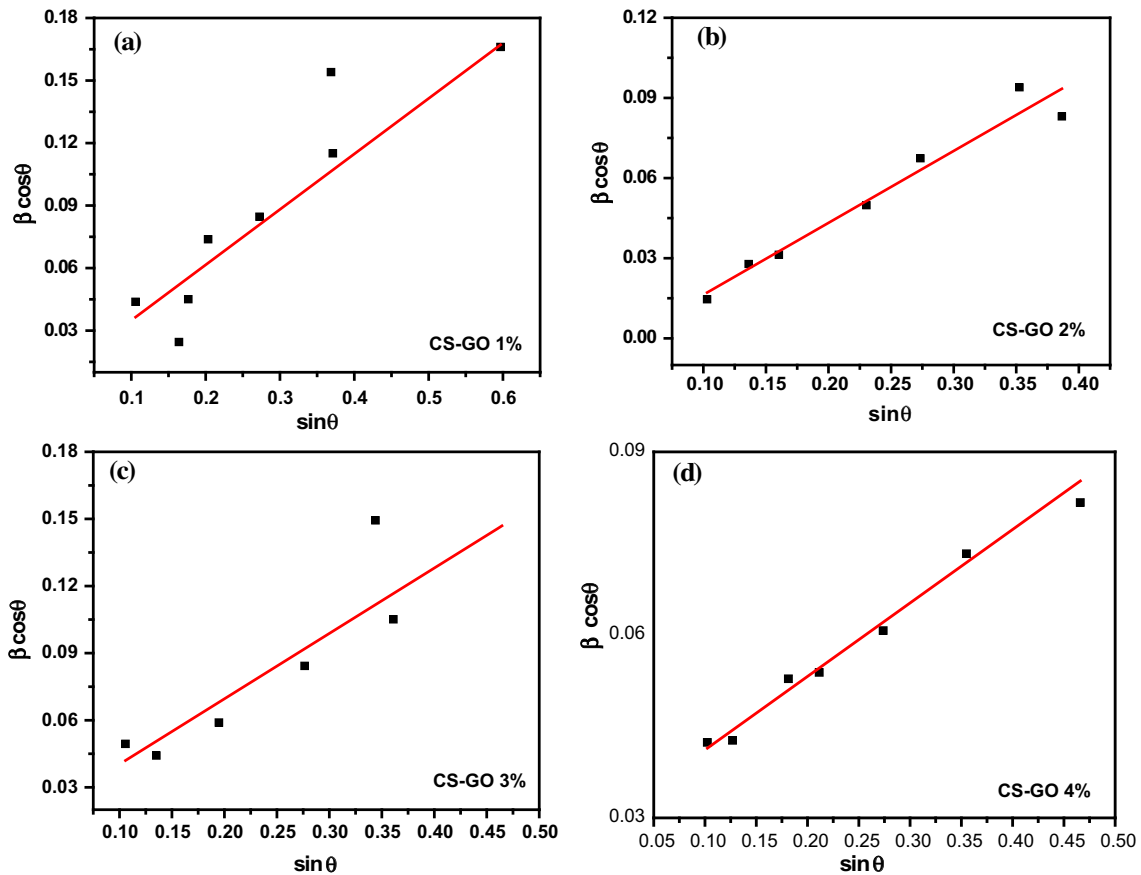


Figure 7 W–H plots for prepared freestanding films of CS-GO polymer nanocomposites.

Table 1 Details of crystallite size and produced micro-strain in CS-GO PNCs

Sample	CS wt%	GO wt%	Crystallite size (nm)	Micro-strain ($\times 10^{-3}$)
CS-GO 1%	0.99	0.01	11.4	26.61
CS-GO 2%	0.98	0.02	12.6	29.61
CS-GO 3%	0.97	0.03	13.2	32.29
CS-GO 4%	0.96	0.04	16.8	39.11

acts as a grain growth promoter, and it results in increasing the crystallite size. However, as the filler promotes the crystallization process, it produces increase of micro-strain in the sample.

Analysis of FTIR spectra

The involvement of the functional groups in the formation of CS-GO novel biocompatible nanocomposite has been explained through FTIR. For the prepared samples of nanocomposites, the FTIR spectra were recorded with the help of IR spectrophotometer (Bruker model α -T). The recorded spectra are shown in Fig. 8. On adding GO to

chitosan, an amide linkage is formed between the -COOH group of GO and -NH_2 group of chitosan, which can be confirmed by FTIR spectra. The dominant peaks observed at 1035 cm^{-1} , 1225 cm^{-1} , 1623 cm^{-1} and 1739 cm^{-1} in the spectrum of GO attributes to the stretching vibration of C–O–C bonds of epoxy groups, C–OH bonds, un-oxidized C=C bonds of graphene oxide and stretching vibrations of C=O bonds associated with the carboxylic and carbonyl moieties of GO, respectively [66]. Further, the dominant peaks observed in the spectrum of chitosan are at 1653 cm^{-1} and 1526 cm^{-1} , which corresponds to the stretching vibration of C=O of -NHCO- and the N–H bending of NH_2 , respectively. In the GO-CS

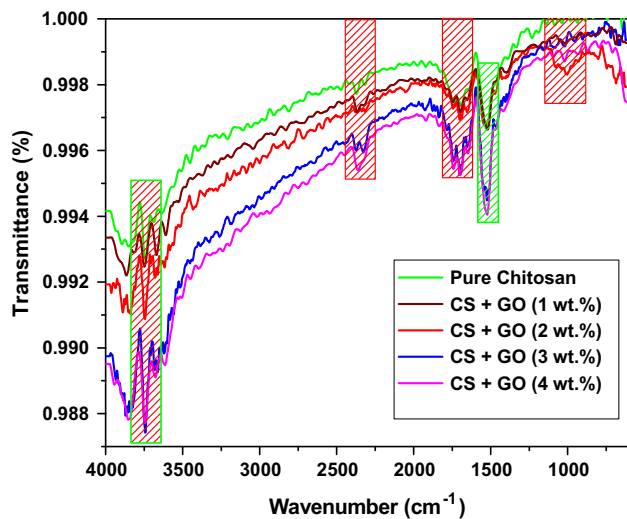


Figure 8 Recorded FTIR spectra of CS-GO polymer nanocomposites.

PNCs spectra, the peak at 1526 cm^{-1} becomes prominent showing the formation of an amide bonds. The two bands appear as a result of coupling of two vibrations in the component C–N–H, one N–H bending (amide II band) at 1693 cm^{-1} and the other C–N stretching (amide III band) at 1742 cm^{-1} . Disappearance of the bands attributed to the C=O of carboxylic group confirms the involvement of –COOH group of GO in the bond formation. Disappearance of two bands in the region between 3200 cm^{-1} and 3600 cm^{-1} attributed to the –NH_2 of CS further confirms the formation of amide linkage between –NH_2 of CS and –COOH of GO. Thus, the data obtained for the CS-GO nanocomposites clearly indicates the formation of a new covalent bond formed between the carboxylic acid of GO and NH_2 of chitosan. On increasing the concentration of GO in the CS-GO PNCs, the peaks at 1653 cm^{-1} and 1594 cm^{-1} becomes more prominent showing the increase of the amide linkages in the CS-GO PNCs, which again confirms the reaction between the NH_2 of chitosan and carboxyl of GO. The peaks observed for pure GO, pure CS and for the prepared CS-GO nanocomposites are summarized in Table 2. The described peaks for all samples of CS-GO PNCs (with 1, 2, 3 and 4 wt% of GO) are shown by the shaded region in Fig. 8. From Fig. 8, it is also clear that the transmittance value is shifted downwards with increasing the GO content in the nanocomposites.

Analysis of Raman spectra

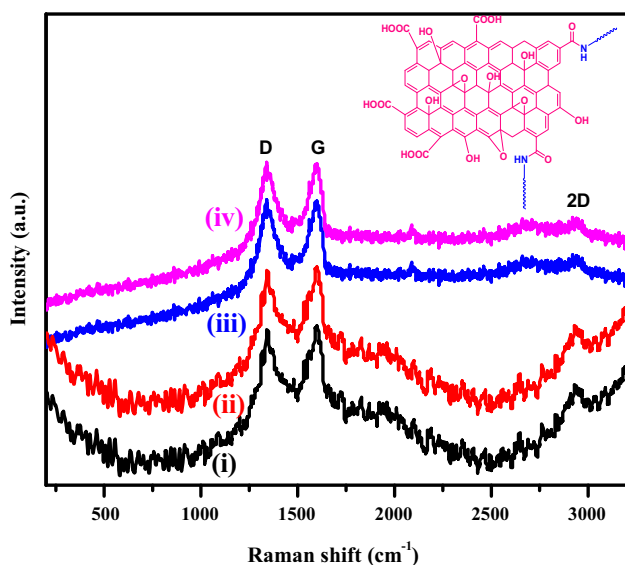
In order to study the characteristic effect of interactions among the components and effects of bonding in the synthesized nanocomposites, so-called standard tool “Raman spectroscopy” can be utilized. For the prepared CS-GO PNCs, the Raman spectra were recorded covering the wave numbers ranging from 50 to 3500 cm^{-1} by using micro-Raman spectrometer (DXRxi, Raman Imaging\Microscope ThermoScientific). In this micro-Raman spectrometer, the laser of 532 nm was used as an excitation source. The recorded Raman spectra of CS-GO PNCs are shown in Fig. 9. The chemical structure of the synthesized CS-GO PNC is shown in the inset of Fig. 9. In Fig. 9, the numbers (i), (ii), (iii) and (iv) represent the spectra of CS-GO PNCs for the 1, 2, 3 and 4 wt% of GO, respectively.

Before the analysis of Raman spectra, the Raman spectra of pure chitosan and pure GO were studied in the previous reported literature. According to it, the Raman spectrum of pure chitosan shows that the pure chitosan is a poor scatterer with a very low Raman cross section [67], and the Raman peaks due to chitosan were obtained at 899, 1110 and 1378 cm^{-1} [68]; instead, the Raman spectra of GO displayed three bands, i.e., D, G and 2D (D + G). These bands are visible at 1348.31, 1594.19 and 2930.13 cm^{-1} , respectively [69]. The occurrence of 2D band supports the presence of a higher disorder structure of graphene oxide and thus becomes responsible for dispersive nature of GO [70]. However, in the Raman spectra of CS-GO PNCs with different wt% of GO, three bands (D, G, and 2D) can clearly be seen, see Fig. 9.

In these spectra, the D and G bands are strong, while the 2D band is less intense. In the spectra of CS-GO PNCs, the intense D and G bands correspond to ~ 1346 and 1604 cm^{-1} , respectively, while the 2D band is at $\sim 2946\text{ cm}^{-1}$. The Raman peaks corresponding to these bands can be referred as the characteristics peaks of the CS-GO PNCs. The close comparison of Raman spectra of pure GO and synthesized CS-GO PNCs confirms that the D, G and 2D bands of the pure GO and the prepared nanocomposites are almost matched. Further, the positions of D, G and 2D bands in the spectra of CS-GO PNCs are found to be very slightly shifted toward smaller wave number with increasing the wt% of GO in nanocomposites. This shifting is due to the presence

Table 2 Functional groups present in pure GO, CS and CS-GO PNCs

S. no.	Assignments	Observed wave number for GO (cm ⁻¹)	Observed wave number for CH (cm ⁻¹)	Observed wave number for CH-GO PNCs (cm ⁻¹)
1	C–O–C stretching	1035	1038	1036
2	C–N stretching vibration	–	1270	–
3	C–OH stretching	1225	1003	1092
4	N–H bending	–	1526	1526
5	C=C stretching	1599	–	–
6	C=O stretching vibration (amide group)	–	1653	1693
7	C–H–N stretching	–	–	1693 and 1742 (coupling of two vibrations)
8	C=O stretching vibration (carboxylic group)	1739	–	–
9	N–H stretching vibration due to -NH ₂	–	3617	–
10	N–H stretching vibration due to -NH of amide	–	3431	3453
11	O–H stretching	3354	3744 (free OH)	3742 (free OH)

**Figure 9** Recorded Raman spectra of CS-GO polymer nanocomposites.

of the matched D, G and 2 D bands in GO. The interesting feature of Raman spectra of CS-GO PNCs is that the less intense 2D band of the CS-GO nanocomposite is enhanced with increasing the GO concentration in the nanocomposites. In the spectra of CS-GO PNCs, the presence of the D band shows the presence of defect sites associated with vacancies and grain boundaries which create the deformation or disorder in the structure. This disorder regularly arises due to the vibration of out-plane sp^2 hybridized carbon (out phase vibrations) surrounding defects or amorphous carbon species. Further, the presence of

the G band represents the ordered graphene structure which is originated from the vibrations of in-plane sp^2 hybridized carbon atoms (in-phase vibrations), and thus, the G-band is credited to the first order scattering of the E_{2g} phonons of the sp^2 hybridized bonds in the material structure. The presence of less intense 2D band signifies the second order of the vibrational mode. Such facts about D, G and 2D bands have also been explained in reported literature [71–76]. Apart from this, the intensity ratios of D and G bands for all the prepared nanocomposites have also been determined. From the calculations, it was found that the intensity ratios (I_D/I_G) for the CS-GO PNCs with 1, 2, 3 and 4 wt% of GO are obtained as ~ 0.9621 , 0.9744 , 0.9937 and 0.9941 , respectively. Thus, this result shows that the intensity ratio (I_D/I_G) is continuously increased with increasing GO concentration. This increase in the (I_D/I_G) ratio is due to the additional defects which occur through electrostatic attraction and availability of several sp^2 hybridized atoms surrounding these defects. In addition, the intensity ratio (I_D/I_G) for the pure GO is ~ 0.93 , which is lower than that of CS-GO PNCs, as mentioned above. The higher values of (I_D/I_G) for the CS-GO PNCs indicate that the sp^3 localized defects are present within the sp^2 carbon atoms which take place via reduction of the exfoliated GO [77].

Surface morphology using SEM

The dispersion and distribution of GO sheets in the nanocomposites were confirmed by using field

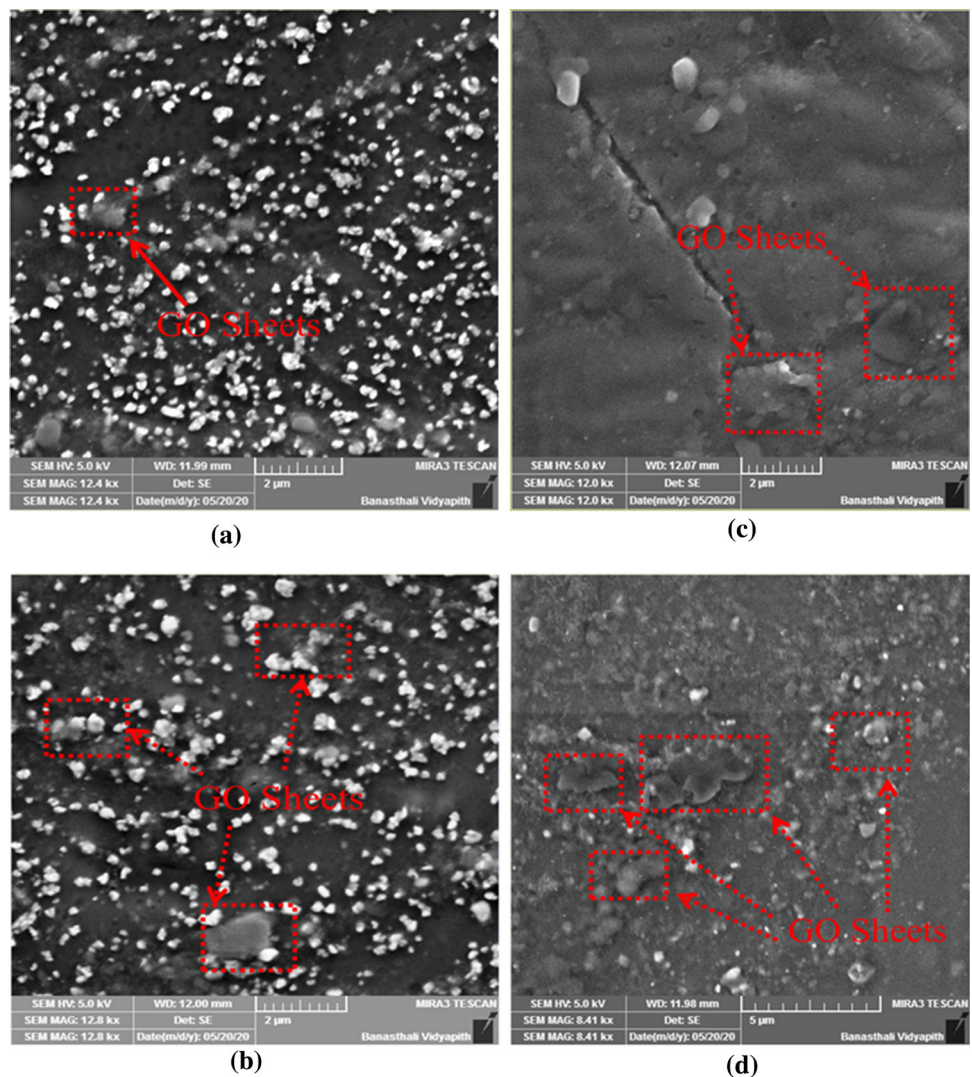
emission scanning electron microscope (FESEM, MIRA3TESCAN). These images clearly indicate the uniform dispersion of GO sheets having micron size in CS matrix. The presence of GO sheets has been shown in rectangle box in Fig. 10. From Fig. 10, it is also noticed that the agglomeration among the grains were found, with increasing content of GO nano-filler in CS polymer matrix.

UV-Vis absorption spectra analysis

The optical properties of the prepared CS-GO PNCs were determined through recording of the optical absorption spectra of the all samples by using UV-Vis-NIR spectrophotometer (PerkinElmer, lambda 750) in the absorbance mode. From the recorded spectra, the optical absorption band edges have been

determined, and optical band gaps of the prepared CS-GO PNCs have been estimated by using Tauc's relation, which is very convenient method of determining the optical band gap [78–81]. In Fig. 11, the optical absorption edge calculated for all the samples of nanocomposites with the GO content of 1 wt%, 2 wt%, 3 wt% and 4 wt% is shown. Again from Fig. 11, it can be predicted that the optical absorption band edge shows a redshift by a smaller magnitude with increasing GO content. For the CS-GO PNCs, the optical absorption edge is found in the UV region, i.e., $\lambda \sim 319$ nm. This means that all the photons above this threshold wavelength will be absorbed by the freestanding film of CS-GO nanocomposite, while below this wavelength all the incident photons will be transmitted.

Figure 10 SEM images showing the presence GO sheets in CS-GO PNCs with GO **a** 1 wt%, **b** 2 wt%, **c** 3 wt% and **d** 4 wt%.



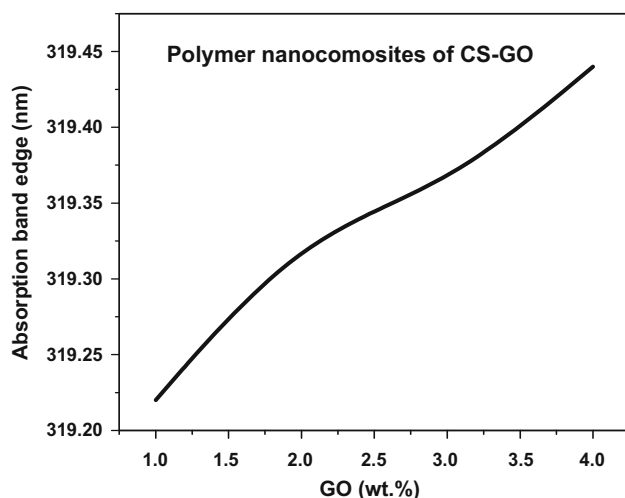


Figure 11 Effect of GO content on absorption band edge of CS-GO PNCs.

Again from the optical absorption data, the graphs between $(\alpha hv)^2$ and (hv) for the prepared samples of CS-GO PNCs were plotted, and from these graphs the extrapolation of the linear least squares fit of α^2 to zero, we got the optical band gap. Thus, the determined optical band gap for all the samples with variation in GO content is plotted in Fig. 12. From Fig. 12, it can be confirmed that the value of the optical band gap of CS-GO nanocomposites is constantly reduced on rising the concentration of GO. Such an orderly decrease in the optical band gap of the prepared CS-GO nanocomposites with the increase in amount of GO points toward the enhancement in the structural disorder of the chitosan polymer matrix with increasing amount of GO.

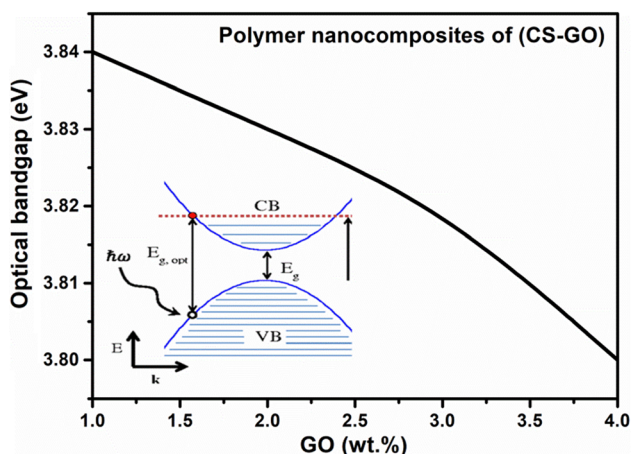


Figure 12 Variation in optical band gap with variation in GO concentration in CS-GO PNCs.

The structural disorder in the polymer matrix due to GO mixing can also be confirmed by the analysis of XRD results, which have shown the produced micro-strain and modification in the crystallite size (see Table 1) due to mixing and increasing the GO contents. Further, the orderly drop in the optical band gap is based on the fact that the mixing of GO in the polymer matrix can generate new states within the band gap, which facilitate the motion of electrons from the valence bands to new produced local states of the conduction band. Moreover, the increased amount of GO in the polymer can produce more and more states due to which the optical band gap is continuously reduced.

Electrical properties

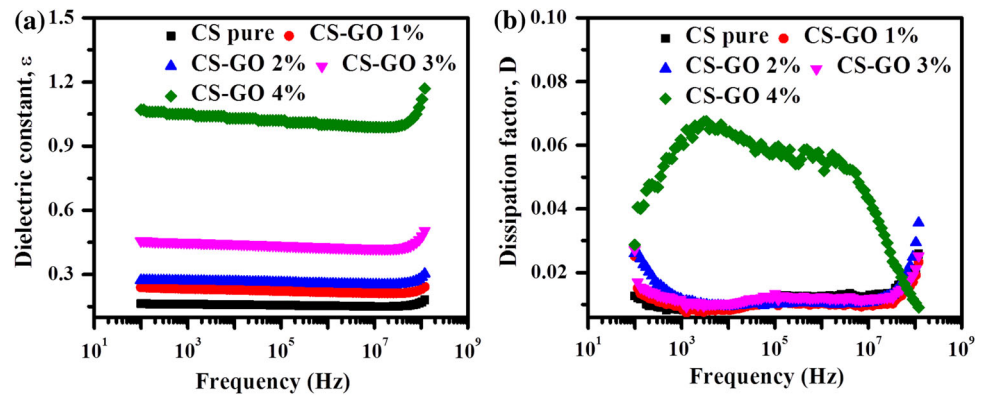
In the electrical properties, we have measured the dielectric constant, dissipation factor and electrical conductivity of the prepared CS-GO PNCs at room temperature in the frequency range 50 kHz–120 MHz using Wayne Kerr 6500B precision impedance analyzer.

Dielectric analysis

The dielectric properties of the prepared PNCs were analyzed at room temperature as a function of the frequency. Figure 13a illustrates the variation of the dielectric constant at room temperature for all compositions. The dielectric properties of materials are derived from the contribution of four forms of polarizations, which are, actually, interfacial polarization, orientational polarization, ionic polarization and electronic polarization [82–84]. Interfacial polarization was present in the frequency range from 1 mHz to 10^3 Hz; orientational polarization was found to be active in the frequency range from 10^3 to 10^6 Hz; ionic polarization between 10^6 and 10^9 Hz and finally electronic polarization above 10^9 Hz was found [83–87].

Based on the available frequency range, only three forms of polarization in the prepared composites of CS-GO films are expected to be present. The dielectric constant shows that it is going to decrease with increasing frequency up to 10^7 Hz, while it starts to be raised above than 10^7 Hz. To understand the dielectric properties of CS-GO composite, the chemical structure of chitosan and graphene has been taken into account. In the case of interfacial

Figure 13 Behaviors of
a dielectric constant;
b dissipation factor of CS-GO
 PNCs.



polarization, when two different regions with varying in their conductivity segregated at the boundary, it results in a high value of dielectric constant due to the absence of boundary in PNCs. Moreover, the presence of ns^2 electron of carbon in graphene and delocalized electron of chitosan formed a dipole that is situated far apart from each other. So, the possibility of the response of dipole in the ac field is slightly difficult, and therefore, the dielectric constant has been decreased up to 10^7 Hz. The presence of ns^2 electron in graphene and delocalized electron in chitosan ionizes as the frequency increases and contributing to increasing the ionic polarization. Therefore, the dielectric constant has been found to be increased. The dielectric constant of pure CS sample is found to be lower and found to be raised with the incorporation of GO in the matrix of chitosan. The concentration of the ns^2 electron of carbon in graphene is increased with increasing the content of GO in the nanocomposites, which might be a possible reason for this variation.

The variation in dissipation factor of prepared PNCs has been shown as a function of frequency at room temperature in Fig. 13 (b). The dissipation factor of PNCs is increased from 0.01267 for Pure CS to 0.02867 for CS-GO 4 wt%. The dissipation factor results due to dc conduction in the sample. In the present case, with increasing GO content in PNCs, the electronic conduction takes place via the ns^2 electron of graphene, which increases and results in higher dc conduction in the sample. The frequency dependence of the dissipation factor follows a similar trend for the nanocomposites of CS-GO up to 3 wt% of GO, while slightly different for CS-GO nanocomposite with 4 wt% of GO. The dissipation factor shows three active regions from sample CS to CS-GO 3 wt% such as:

- (i) Initially, the dissipation factor decreases to a particular value with increasing frequency up to 10^3 Hz.
- (ii) In the second region, the dissipation factor found to be increased with increasing frequency from 10^3 to 10^7 Hz.
- (iii) In the third region again, the dissipation factor found to be shoot up to a tremendous value.

Since, below 10^3 Hz, interfacial polarization takes place, the charge carriers of graphene and chitosan are segregated by a boundary. Due to this segregation of charge carriers, no dc conduction takes place, and the dissipation factor found to be decreased [process (i)]. However, in frequency range 10^3 – 10^7 Hz, the orientational polarization takes place. In this process, the charge carriers are migrated by the orientation. Through this, a small amount of dc conduction takes place and results to be increased dissipation factor [process (ii)]. In the present case, the dipole is formed between the dislocated site of chitosan and ns^2 electron of graphene, which made response on the application of the ac electric field. Moreover, above 10^7 Hz, the ionic polarization takes place. The presence of ns^2 electron at graphene results to be ionized with increasing frequency is assigned to process (iii). However, a weak relaxation peak is observed in the variation of dissipation factor at 1.34×10^5 Hz, 1×10^5 Hz, 8.4×10^4 Hz and 6.6×10^4 Hz for samples CS, CS-GO 1 wt%, CS-GO 2 wt% and Cs-GO 3 wt%, respectively. This relaxation peak is assigned to the orientation of dipole, and the shift toward lower frequency might be due to a decrease in distance between dipole. The variation of the dissipation factor of sample CS-GO 4 wt% shows two relaxation peaks at 3.3×10^3 Hz and 9.75×10^5 Hz. These

relaxation peaks are assigned to the orientation of dipole and ionization of the ns^2 electron. Further, to reconfirm the dc conduction, electrical conductivity of PNCs has been studied and discussed in the subsequent section.

Electrical conductivity

Furthermore, to reaffirm the dc conduction in the CS-GO PNCs, the alternating current (AC) conductivity of samples is plotted in Fig. 14. It shows that, with increasing the frequency, the conductivity is increased linearly. The present value of conductivity is higher compared to the literature, which suggests that the conduction takes place either by defective electron or free electron in the sample [88]. The variation of ac conductivity shows two regions, in the first region the conductivity is independent of frequency termed as dc conductivity (σ_{dc}). In the second region, the conductivity increases linearly with frequency termed as ac conductivity (σ_{ac}). The frequency at which the transition between frequency independence conduction to frequency-dependent conduction takes place is known as hopping frequency (f_H). According to Johnscher's power law, the ac conductivity has been given as following [63]:

$$\sigma_{ac} = \sigma_{dc} \left(1 + \frac{f}{f_H} \right)^n \quad (6)$$

where n is called an index parameter. By employing the fitting of Eq. (6) to experimental data, we obtained the value of σ_{dc} , f_H and n . The value of dc conductivity is found to be increased with increasing the content of GO. This increase in conductivity is

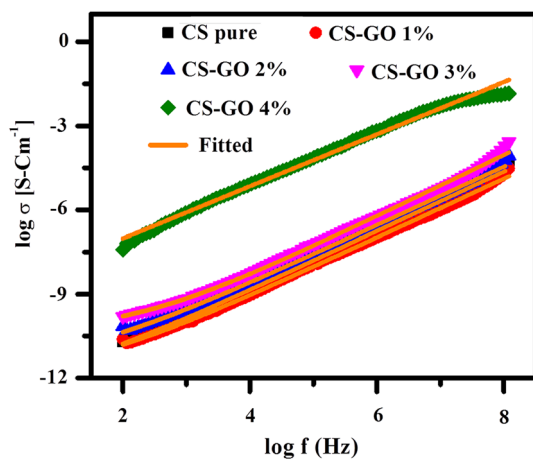


Figure 14 Variation in electrical conductivity in CS-GO PNCs.

directly related to the concentration of the mobile charge carrier of the ns^2 electron of GO. However, the value of σ_{dc} , f_H and n for all samples are given in Table 3.

However, the value of n between 0 and 1 for all samples suggests that the conduction in these samples takes place by direct as well as hopping of charge carrier between the respective sites. A higher value of hopping frequency is also increased with increasing content of GO. Increasing the content of GO has further increased the individual sites of hopping. As the number of hopping sites increases, the conductivity results to be increased with increasing frequency as well as the content of GO. However, the similar kind of variation in electrical conductivity has also been reported in PANI-MWCNTs and SPAN-MWCNTs nanocomposites by Reddy et al. [89,90]. The higher value of electrical conductivity at high frequency makes it a suitable and potential candidate for high frequency-based device applications.

Current–Voltage (I–V) study

The I–V characteristics of prepared thin films of CS-GO PNCs using four probe systems were recorded within voltage range from -2 to $+2$ V using Keithly Sourcemeter (Keithley 2010). Figure 15 shows the I–V curve of CS-GO PNCs with varying GO nano-filler concentrations in CS polymer matrix. The current value in comparison to applied voltage exhibits a linear behavior for all samples, suggesting the existence of Ohmic conduction in PNCs [90]. As the concentration of GO in the polymer matrix of CS increased, the current value was found to be 0.89 mA, 0.67 mA, 1.03 mA, 0.68 mA, 0.67 mA at the implementation voltage of 1.015 V for samples of pure CS, CS-GO 1 wt%, CS-GO 2 wt%, CS-GO 3 wt% and CS-GO 4 wt%, respectively. The rising in net

Table 3 Estimated parameters (σ_{dc} , f_H and n) of CS-GO PNCs

Sample	σ_{dc} (S cm ⁻¹)	f_H (Hz)	n
CS	– 12.42799	4.46409	0.46081
CS-GO 1%	– 11.91225	21.02087	0.45715
CS-GO 2%	– 11.52653	27.45796	0.45458
CS-GO 3%	– 10.37554	159.66091	0.47484
CS-GO 4%	– 7.51419	217.7711	0.50114

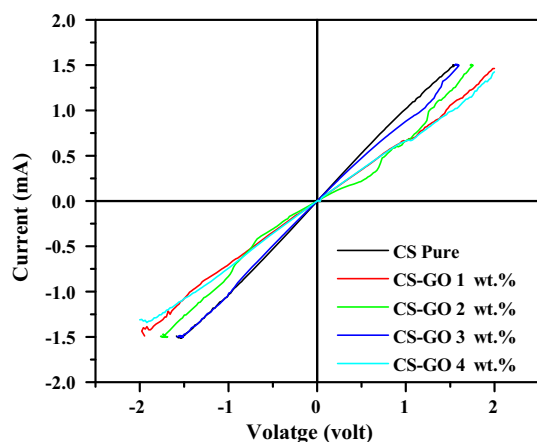


Figure 15 I–V curves of CS-GO PNCs with different GO wt%.

current in prepared PNCs is due to migration of charge carrier through the samples. Since the value of electric current is dependent on the surface area (A), charge carrier concentration (n), drift velocity (v_d) and electronic charge (e) by formula $I = neAv_d$. During the measurement, the surface area of all films was kept constant, so the variations found in the sample might be observed due to change in n and v_d . By incorporating GO in the CS polymer matrix, the electrons can transfer easily from GO to CS, resulting in an increase in value of current [91,92]. From UV–Vis (see Fig. 12) studies of samples, it is clearly observed that the optical band gap becomes narrow with the incorporation of GO, so that the transfer of charges from GO to CS becomes easy. Decrease in the value of current can be understood from the surface morphology as shown in Fig. 10 that dispersion of GO in sample has been found to be agglomerated in CS polymer matrix which results gradual increase of resistance. As, the resistance of sample increases, the drifting of charge carrier is not possible through that channel and results decrease in the value of current. Based on the variation observed in present case between voltage and current, the present material can be used to sense various types of gases like CO_2 , O_2 , NH_3 , etc.

Conclusive remark

The CS-GO PNCs with different GO wt% have been synthesized successfully. The structural geometry, electronic structure and potential distribution have been computed for these PNCs. The crystallized phase of CS-GO has been studied by XRD, which shows that GO dominate over the CS and

modification in crystallite size and presence of micro-strain. The proper formation of PNCs and presence of functional group in the composites have been studied by FTIR and Raman spectroscopic analysis. The FESEM has been used to identify the proper dispersion and distribution of GO sheets. The SEM images reveals the agglomeration among the grains with increasing content of GO nano-filler in CS polymer matrix. Optical absorption edge and band gap analyzed from UV–Vis analysis reveal the semiconducting nature of PNCs. In addition, the optical band gap is tuned with by varying the content of GO in PNCs. This tuning in band gap has also been supported by XRD and computational results. The dielectric constant and dc conductivity are found increased with increasing content of GO in PNCs. In addition, these PNCs have also shown an Ohmic type conduction revealed from the study of I–V characteristics. On the basis of outcomes and analysis, the CS-GO PNC may be utilized in the fabrication of optical and gas sensors, UV detectors and electronic, optoelectronic or electrical devices operating at high frequencies.

Acknowledgements

P. A. Alvi is grateful to UGC-DAE Kolkata center for supporting the work through sanctioned project (UGC-DAE-CSR-KC/CRS/19/RC14/0992/1027). One of the authors (Vimala Dhayal) is thankful to University of Rajasthan for providing Dielectric measurement facility. Authors are also grateful to DST, Govt. of India for providing the support in terms of CURIE scheme sanctioned to the Banasthali Vidyapith.

Compliance with ethical standards

Conflict of interest The authors declare that they have no conflict of interest.

References

- [1] Wang SH, Han MY, Huang DJ (2009) Nitric oxide switches on the photoluminescence of molecularly engineered quantum dots. *J Am Chem Soc* 131:11692–11694
- [2] Michalet X, Pinaud FF, Bentolila LA, Tsay JM, Doose S, Li JJ, Sundaresan G, Wu AM, Gambhir SS, Weiss S (2005) Quantum dots for live cells, in vivo imaging, and diagnostics. *Science* 307:538–544

- [3] Wang Y, Li Z, Wang J, Li J, Lin Y (2011) Graphene and graphene oxide: biofunctionalization and applications in biotechnology. *Trend Biotechnol* 29:205–212
- [4] Li C, Adamcik J, Mezzenga R (2012) Biodegradable nanocomposites of amyloid fibrils and graphene with shape-memory and enzyme-sensing properties. *Nat Nanotechnol* 7:421–427
- [5] Mochalin VN, Gogotsi Y (2009) Wet chemistry route to hydrophobic blue fluorescent nanodiamond. *J Am Chem Soc* 131:4594–4595
- [6] Peng J, Gao W, Gupta BK, Liu Z, Aburto RR, Ge L, Song L, Alemany LB, Zhan X, Gao G, Vithayathil SA, Kaiparettu A, Marti AA, Hayashi T, Zhu JJ, Ajayan PM (2012) Graphene quantum dots derived from carbon fibers. *Nano Lett* 12:844–849
- [7] Chabba S, Matthews GF, Netravali AN (2005) ‘Green’ composites using cross-linked soy flour and flax yarns. *Green Chem* 7:576–581
- [8] Yoo BM, Shin HJ, Yoon HW, Park HB (2014) Graphene and graphene oxide and their uses in barrier polymers. *J Appl Polym Sci* 131(1):39628
- [9] Cheng C, Li S, Thomas A, Kotov NA, Haag R (2017) Functional graphene nanomaterials based architectures: biointeractions, fabrications, and emerging biological applications. *Chem Rev* 117(3):1826–1914
- [10] Ravi Kumar MNV (2000) A review of chitin and chitosan applications. *React Funct Polym* 46(1):1–27
- [11] Khichar KK, Dangi SB, Dhayal V, Kumar U, Hashmi SZ, Sadhu V, Choudahry BL, Kumar S, Kaya S, Kuznetsov AE, Dalela S, Gupta SK, Alvi PA (2020) Structural, optical, and surface morphological studies of ethyl cellulose/graphene oxide nanocomposites. *Polym Compos* 10:1–11. <https://doi.org/10.1002/pc.25576>
- [12] Dong X, Wei C, Liang J, Liu T, Kong D, Lv F (2017) Thermosensitive hydrogel loaded with chitosan-carbon nanotubes for near infrared light triggered drug delivery. *Colloids Surf B* 154:253–262
- [13] Benucci I, Liburdi K, Cacciotti I, Lombardelli C, Zappino M, Nanni F, Esti M (2018) Chitosan/clay nanocomposite films as supports for enzyme immobilization: an innovative green approach for winemaking applications. *Food Hydrocolloids* 74:124–131
- [14] Al-Naamani L, Dobretsov S, Dutta J (2010) Chitosan-zinc oxide nanoparticle composite coating for active food packaging applications. *Innov Food Sci Emerg Technol* 38:231–237
- [15] Reddy KR, Park W, Sin BC, Noh J, Lee Y (2009) Synthesis of electrically conductive and superparamagnetic monodispersed iron oxide-conjugated polymer composite nanoparticles by in situ chemical oxidative polymerization. *J Colloid Interface Sci* 335(1):34–39
- [16] Reddy KR, Lee KP, Iyengar AG (2007) Synthesis and characterization of novel conducting composites of Fe₃O₄ nanoparticles and sulfonated polyanilines. *J Appl Polym Sci* 104(6):4127–4134
- [17] Reddy KR, Lee KP, Gopalan AI, Kang HD (2007) Organosilane modified magnetite nanoparticles/poly (aniline-co-o/m-aminobenzenesulfonic acid) composites: synthesis and characterization. *React Funct Polym* 67(10):943–954
- [18] Reddy KR, Lee KP, Gopalan AI, Showkat AM (2007) Synthesis and properties of magnetite/poly(aniline-co-8-amino-2-naphthalenesulfonic acid) (SPAN) nanocomposites. *Polym Adv Technol* 18(1):38–43
- [19] Reddy KR, Lee KP, Kim JY, Lee Y (2008) Self-assembly and graft polymerization route to monodispersed Fe₃O₄@-SiO₂-polyaniline core-shell composite nanoparticles: physical properties. *J Nanosci Nanotechnol* 8(11):5632–5639
- [20] Reddy KR, Lee KP, Gopalan AI (2007) Novel electrically conductive and ferromagnetic composites of poly (aniline-co-aminonaphthalenesulfonic acid) with iron oxide nanoparticles: synthesis and characterization. *J Appl Polym Sci* 106(2):1181–1191
- [21] Dakshayini BS, Reddy KR, Mishra A, Shetti NP, Malode SJ, Basu S, Naveen S, Raghu AV (2019) Role of conducting polymer and metal oxide-based hybrids for applications in amperometric sensors and biosensors. *Microchem J* 127:7–24
- [22] Ajayan PM, Schadle LS, Giannaris C, Rubio A (2000) ‘Single-walled carbon nanotube-polymer composites: strength and weakness. *Adv Mater* 12:750–753
- [23] Salavagione HJ, Martinez G, Ellis G (2011) Recent advances in the covalent modification of graphene with polymers. *Macromol Rapid Commun* 32:1771–1789
- [24] Fazil S, Bangesh M, Rehman W, Liaqat K, Saeed S, Sajid M, Waseem M, Shakeel M, Bibi I, Guo C-Y (2019) Mechanical, thermal, and dielectric properties of functionalized graphene oxide/polyimide nanocomposite films. *Nanomater Nanotechnol* 9:1–8
- [25] Reddy KR, Sin BC, Ryu KS, Kim JC, Chung H, Lee Y (2009) Conducting polymer functionalized multi-walled carbon nanotubes with noble metal nanoparticles: synthesis, morphological characteristics and electrical properties. *Synth Met* 159(7–8):595–603
- [26] Khan MU, Reddy KR, Snguanwongchai T, Haque E, Gomes VG (2016) Polymer brush synthesis on surface modified carbon nanotubes via in situ emulsion polymerization. *Colloid Polym Sci* 294(10):1599–1610

- [27] Lerf A, Heyong H, Forster M, Klinowski J (1998) Structure of graphite oxide revisited. *J Phys Chem B* 102:4477–4482
- [28] Lomeda JR, Doyle CD, Kosynkin DV, Hwang W-F, Tour JM (2008) Diazonium functionalization of surfactant-wrapped chemically converted graphene sheets. *J Am Chem Soc* 130:16201–16206
- [29] Qi X, Pu KY, Zhou X, Li H, Liu B, Boey F, Huang W, Zhang H (2010) Conjugated-polyelectrolyte functionalized reduced graphene oxide with excellent solubility and stability in polar solvents. *Small* 6:663–669
- [30] Alvi PA, Hashmi SZ, Dalela S, Rahman F (2011) Mathematical simulation of graphene with modified C–C bond length and transfer energy. *J Nanoelectron Phys* 3(3):42
- [31] Smith AT, LaChance AM, Zeng S, Liu B, Sun L (2019) Synthesis, properties, and applications of graphene oxide/reduced graphene oxide and their nanocomposites. *Nano Mater Sci* 1(1):31–47
- [32] Lee C, Wei X, Kysar JW, Hone J (2008) Measurement of the elastic properties and intrinsic strength of monolayer graphene. *Science* 321(5887):385–388
- [33] Kim M, Lee C, Jang J (2014) Fabrication of highly flexible, scalable, and high performance supercapacitors using polyaniline/reduced graphene oxide film with enhanced electrical conductivity and crystallinity. *Adv Funct Mater* 24(17):2489–2499
- [34] Hassan M, Reddy KR, Haque E, Faisal SN, Ghasemi S, Minett AI, Gomes VG (2014) Hierarchical assembly of graphene/polyaniline nanostructures to synthesize free-standing supercapacitor electrode. *Compos Sci Technol* 98:1–8
- [35] Lee YR, Kim SC, Lee HI, Jeong HM, Raghu AV, Reddy KR, Kim BK (2011) Graphite oxides as effective fire retardants of epoxy resin. *Macromol Res* 19(1):66–71
- [36] Son DR, Raghu AV, Reddy KR, Jeong HM (2016) Compatibility of thermally reduced graphene with polyesters. *J Macromol Sci B* 55(11):1099–1110
- [37] Han SJ, Lee HI, Jeong HM, Kim BK, Raghu AV, Reddy KR (2014) Graphene modified lipophilically by stearic acid and its composite with low density polyethylene. *J Macromol Sci B* 53(7):1193–1204
- [38] Choi SH, Kim DH, Raghu AV, Reddy KR, Lee H-I, Yoon KS, Jeong HM, Kim BK (2012) Properties of graphene/waterborne polyurethane nanocomposites cast from colloidal dispersion mixtures. *J Macromol Sci B* 51(1):197–207
- [39] Cui Y, Kundalwal SI, Kumar S (2016) Gas barrier performance of graphene/polymer nanocomposites. *Pergamon* 98:313–333
- [40] Ghauri FA, Raza MA, Baig MS, Ibrahim S (2017) Corrosion study of the graphene oxide and reduced graphene oxide-based epoxy coatings. *Mater Res Express* 4(12):125601–125601
- [41] Tan B, Thomas NL (2016) A review of the water barrier properties of polymer/clay and polymer/graphene nanocomposites. *J Membr Sci* 514:595–612
- [42] Nair JR, Francesca C, Arefeh K, Margherita M, Dominic B, Rongying L, Bella F, Meligrana G, Fantini S, Simonetti E, Appetecchi GB (2019) Room temperature ionic liquid (RTIL)-based electrolyte cocktails for safe, high working potential Li-based polymer batteries. *J Power Sources* 412:398–407
- [43] Scalia A, Bella F, Lamberti A, Gerbaldi C, Tresso E (2019) Innovative multipolymer electrolyte membrane designed by oxygen inhibited UV-crosslinking enables solid-state in plane integration of energy conversion and storage devices. *Energy* 166:789–795
- [44] LefrançoisPerreault L, Colò F, Meligrana G, Kim K, Fiorilli S, Bella F, Nair JR, Vitale-Brovarone C, Florek J, Kleitz F, Gerbaldi C (2018) Nanostructured li-ion batteries: spray-dried mesoporous mixed Cu–Ni oxide@graphene nanocomposite microspheres for high power and durable li-ion battery anodes. *Adv Energy Mater* 8(35):1870150
- [45] Piana G, Ricciardi M, Bella F, Cucciniello R, Proto A, Gerbaldi C (2020) Poly(glycidyl ethers) recycling from industrial waste and feasibility study of reuse as electrolytes in sodium-based batteries. *Chem Eng J* 382:122934
- [46] Piana G, Bella F, Geobaldo F, Meligrana G, Gerbaldi C (2019) PEO/LAGP hybrid solid polymer electrolytes for ambient temperature lithium batteries by solvent-free, “one pot” preparation. *J Energy Storage* 26:100947
- [47] Falco M, Castro L, Nair JR, Bella F, Bardé F, Meligrana G, Gerbaldi C (2019) UV-cross-linked composite polymer electrolyte for high-rate, ambient temperature lithium batteries. *ACS Appl Energy Mater* 2(3):1600–1607
- [48] Deyab MA, Mele G (2020) Stainless steel bipolar plate coated with polyaniline/Zn-Porphyrin composites coatings for proton exchange membrane fuel cell. *Sci Rep* 10:3277
- [49] Perumal S, Atchudan R, Yoon DH, Joo J, Cheong IW (2020) Graphene oxide-embedded chitosan/gelatin hydrogel particles for the adsorptions of multiple heavy metal ions. *J Mater Sci* 55:9354–9363. <https://doi.org/10.1007/s10853-020-04651-1>
- [50] Frisch MJ, Trucks GW, Schlegel HB, Scuseria GE, Robb MA, Cheeseman JR, Scalmani G, Barone V, Mennucci B, Petersson GA et al (2010) Gaussian 09, Revision B.01. Gaussian Inc., Wallingford
- [51] Becke AD (1993) Density-functional thermochemistry. III. The role of exact exchange. *J Chem Phys* 98:5648–5652
- [52] Parr RG, Yang W (1989) Density-functional theory of atoms and molecules. Oxford University Press, Oxford

- [53] McLean AD, Chandler GS (1980) Contracted Gaussian-basis sets for molecular calculations. 1. 2nd row atoms, $Z = 11-18$. *J Chem Phys* 72:5639–5648
- [54] Raghavachari K, Binkley JS, Seeger R, Pople JA (1980) Self-consistent molecular orbital methods. 20. Basis set for correlated wave-functions. *J Chem Phys* 72:650–654
- [55] Reed AE, Curtiss LA, Weinhold F (1988) Intermolecular interactions from a natural bond orbital, donor-acceptor viewpoint. *Chem Rev* 88:899–926
- [56] Reed AE, Weinstock RB, Weinhold F (1985) Natural-population analysis. *J Chem Phys* 83:735–746
- [57] Schaftenaar G, Noordik JH (2000) Molden: a pre- and post-processing program for molecular and electronic structures. *J Comput Aided Mol Des* 14:123–134
- [58] Avogadro: an open-source molecular builder and visualization tool. Version 1.1.1. <https://avogadro.cc/>
- [59] Hanwell MD, Curtis DE, Lonie DC, Vandermeersch T, Zurek E, Hutchison GR (2012) Avogadro: an advanced semantic chemical editor, visualization, and analysis platform. *J Cheminform* 4:17
- [60] Li W, Zhiwei Xu, Chen L, Mingjing Shan Xu, Tian CY, Lv H, Qian X (2014) A facile method to produce graphene oxide-g-poly (L-lactic acid) as an promising reinforcement for PLLA nanocomposites. *Chem Eng J* 237:291–299
- [61] Dey SC, Al-Amin M, Rashid TU, Sultan MZ, Ashaduzzaman M, Sarker M, Shamsuddin SM (2016) Preparation, characterization and performance evaluation of chitosan as an adsorbent for remazol red. *Int J Latest Res Eng Technol* 2(2):52–62
- [62] Kumar U, Ansaree J, Upadhyay S (2017) Structural and optical characterizations of BaSnO₃ nanopowder synthesized by aqueous sol-gel method. *Process Appl Ceram* 11(3):177–184
- [63] Kumar U, Upadhyay S (2019) Structural, optical and electrical properties of Ruddlesden popper oxide Ba₂SnO₄. *J Electron Mater* 48(8):5279–5293
- [64] Callister WD Jr, Rethwisch DG (2020) Callister's materials science and engineering. Wiley, New York
- [65] Liu X, Sheng Y, Dongliang Wu, Zhang R, Cui H (2019) Synthesis of PAMAM-GO as new nanofiller to enhance the crystallization properties of polylactic acid. *Mater Lett* 235:27–30
- [66] Marcano DC, Kosynkin DV, Berlin JM, Sinitiskii A, Sun ZZ, Slesarev A, Alemmany LB, Lu W, Tour JM (2010) Improved synthesis of graphene oxide. *ACS Nano* 4:4806–4814
- [67] Correa DS, Tayalia P, Cosendey G, dos Santos Jr DS, Aroca RF, Mazur E, Mendonca CR (2009) Two-photon polymerization for fabricating structures containing the biopolymer chitosan. *J Nanosci Nanotechnol* 9:5845–5849
- [68] Nishad PA, Kumar A, Pillai B, Velmurugan S (2014) Nanotitania-crosslinked chitosan composite as a superior sorbent for antimony (III) and (V). *Carbohydr Polym* 108(8):169–175
- [69] Kim S-G, Park O-K, Lee JH, Ku B-C (2013) Layer-by-layer assembled graphene oxide films and barrier properties of thermally reduced graphene oxide membranes. *Carbon Lett* 14(4):247–250
- [70] Bîru EI, Iovu H (2018) Graphene nanocomposites studied by Raman spectroscopy. In: do Nascimento GM (ed) Raman spectroscopy. IntechOpen, London. <https://doi.org/10.5772/intechopen.73487>
- [71] Kim NH, Kuila T, Lee JH (2013) Simultaneous reduction, functionalization and stitching of graphene oxide with ethylenediamine for composites application. *J Mater Chem A* 1:1349
- [72] Park OK, Hahm MG, Lee S, Joh HI, Na SI, Vajtai R, Lee JH, Ku BC, Ajayan PM (2012) In situ synthesis of thermally reduced graphene oxide conducting nanocomposites. *Nano Lett* 12:1789
- [73] Bustos-Ramírez K, Martínez-Hernández AL, Martínez-Barraera G, de Icaza M, Castañón VM, Velasco-Santos C (2013) Covalently bonded chitosan on graphene oxide via redox reaction. *Materials* 6(3):911–926
- [74] Worsley KA, Ramesh P, Mandal SK, Niyogi S, Itkis ME, Haddon RC (2007) Soluble graphene derived from graphite fluoride. *Chem Phys Lett* 445:51–56
- [75] Park S, An J, Piner RD, Jung I, Yang D, Velamakanni A, Nguyen ST, Ruoff RS (2008) Aqueous suspension and characterization of chemically modified graphene sheets. *Chem Mater* 20:6592–6594
- [76] Kudin KN, Ozbas B, Schniepp HC, Prudhomme RK, Aksay IA, Car R (2008) Raman spectra of graphite oxide and functionalized graphene sheets. *Nano Lett* 8:36–41
- [77] Kumar S, Koh J (2014) Physiochemical and optical properties of chitosan based graphene oxide bionanocomposite. *Int J Biol Macromol* 70:559–564
- [78] Soni S, Vats VS, Kumar S, Dalela B, Mishra M, Meena RS, Gupta G, Alvi PA, Dalela S (2018) Structural, optical and magnetic properties of Fe-doped CeO₂ samples probed using X-ray photoelectron spectroscopy. *J Mater Sci Electron Mater* 29(12):10141
- [79] Muhammad FF, Aziz SB, Hussein SA (2015) Effect of the dopant salt on the optical parameters of PVA: NaNO₃ solid polymer electrolyte. *J Mater Sci Mater Electron* 26:521–529
- [80] Kumari K, Aljawfi RN, Chawla AK, Kumar R, Alvi PA, Alshoaibi A, Vij A, Ahmed F, Abu-Samak M, Kumar S (2020) Engineering the optical properties of Cu doped CeO₂ NCs for application in white LED. *Ceram Int* 46:7482–7488
- [81] Kumar S, Sharma M, Aljawfi RN, Chae KH, Kumar R, Dalela S, Alshoaibi A, Ahmed F, Alvi PA (2020) Tailoring

- the structural, electronic structure, and optical properties of Fe:SnO₂ nanoparticles. *J Electron Spectrosc Relat Phenom* 240:146934
- [82] Nogales A, Ezquerro TA, Rueda DR, Martinez F, Retuert J (1997) Influence of water on the dielectric behaviour of chitosan film. *Colloid Polym Sci* 275(5):419–425
- [83] Kumar U, Upadhyay S (2020) Structural, microstructure, optical, and dielectric properties of Sr_{1.99}M_{0.01}SnO₄ (M: La, Nd, Eu) Ruddlesden–Popper oxide. *J Mater Sci Mater Electron* 3140:1–10
- [84] Hamsan MH, Shujahadeen BA, Azha MAS, Azli AA, Shukur MF, Yusof YM, Muzakir SK, Manan NSA, Kadir MFZ (2020) Solid-state double layer capacitors and protonic cell fabricated with dextran from *Leuconostoc mesenteroides* based green polymer electrolyte. *Mater Chem Phys* 241:122290
- [85] Aziz SB, Hamsan MH, Kadir MFZ, Woo HJ (2020) Design of polymer blends based on chitosan: POZ with improved dielectric constant for application in polymer electrolytes and flexible electronics. *Adv Polym Technol*. <https://doi.org/10.1155/2020/8586136>
- [86] Kumar U, Kumar A, Yadav D, Upadhyay S (2020) Synthesis and characterization of Ruddlesden–Popper system (Ba_{1-x}Sr_x)₂SnO₄. *Mater Charact* 162:110198
- [87] Patsidis AC, Psarras GC (2020) Applications of dielectric. *Polym Multicompon Polym Syst Therm Thermo-Mech Dielectr Anal* 245:118351
- [88] Islam A, Imran Z, Yasin T, Gull N, Khan SM, Shafiq M, Sabir A, Munawar MA, Raza MH, Jamil T (2015) An investigation of AC impedance and dielectric spectroscopic properties of conducting chitosan-silane crosslinked-poly(vinyl alcohol) blended films. *Mater Res* 18(6):1256–1263
- [89] Reddy KR, Sin BC, Yoo CH, Sohn D, Lee Y (2009) Coating of multiwalled carbon nanotubes with polymer nanospheres through microemulsion polymerization. *J Colloid Interface Sci* 340(2):160–165
- [90] Reddy KR, Lee KP, Gopalan AI, Kim MS, Showkat AM, Nho Y (2006) Synthesis of metal (Fe or Pd)/alloy (Fe–Pd)-nanoparticles-embedded multiwall carbon nanotube/sulfonated polyaniline composites by γ irradiation^{*}. *J Polym Sci A Polym Chem* 44(10):3355–3364
- [91] Yeole B, Sen T, Hansora D, Mishra S (2016) Polypyrrole/metal sulphide hybrid nanocomposites: synthesis, characterization and room temperature gas sensing properties. *Mater Res* 19(5):999–1007
- [92] Trigona C, Al-Hamry A, Kanoun O, Baglio S (2018) Hybrid micro electro mechanical sensor based on graphene oxide/polyvinyl alcohol for humidity measurements. *Multidiscip Digit Publ Inst Proc* 2(13):1011

Publisher's Note Springer Nature remains neutral with regard to jurisdictional claims in published maps and institutional affiliations.